

MR. TAEJIN PARK (Orcid ID : 0000-0003-0698-6942)

DR. MARC MACIAS-FAURIA (Orcid ID : 0000-0002-8438-2223)

DR. SHILONG PIAO (Orcid ID : 0000-0001-8057-2292)

Article type : Primary Research Articles

Changes in timing of seasonal peak photosynthetic activity in northern ecosystems

Running Title: Shifting timing of peak plant photosynthesis

Taejin Park^{1,*}, Chi Chen¹, Marc Macias-Fauria², Hans Tømmervik³, Sungho Choi⁴, Alexander Winkler^{5,6}, Uma S. Bhatt⁷, Donald A. Walker⁸, Shilong Piao⁹, Victor Brovkin⁵, Ramakrishna R. Nemani¹⁰, Ranga B. Myneni¹

¹Department of Earth and Environment, Boston University, Boston MA 02215, USA

²School of Geography and the Environment, University of Oxford, Oxford OX1 3QY, UK

³Norwegian Institute for Nature Research, FRAM – High North Research Centre for Climate and the Environment, NO-9296 Tromsø, Norway

This article has been accepted for publication and undergone full peer review but has not been through the copyediting, typesetting, pagination and proofreading process, which may lead to differences between this version and the Version of Record. Please cite this article as doi: 10.1111/gcb.14638

This article is protected by copyright. All rights reserved.

⁴Rhombus Power Inc., NASA Ames Research Park, Moffett Field, CA 94035, USA

⁵Max-Planck-Institute for Meteorology, Bundesstrasse 53, 20146 Hamburg, Germany

⁶International Max-Planck Research School for Earth System Modeling, Bundesstrasse 53,
20146 Hamburg, Germany

⁷Geophysical Institute, University of Alaska Fairbanks, Fairbanks, AK 99775-7320, USA

⁸Institute of Arctic Biology, University of Alaska, Fairbanks, AK 99775-7000, USA

⁹College of Urban and Environmental Sciences, Peking University, Beijing 100871, China

¹⁰NASA Ames Research Center, Moffett Field, CA 94035, USA

*Corresponding author. Email: parktj@bu.edu; Phone: +1 617 893 1988

Key words (6 to 10): photosynthetic seasonality, climate constraint, law of minimum, gross primary productivity, carbon cycle, climate change, remote sensing, eddy-covariance, earth system model

ABSTRACT

Seasonality in photosynthetic activity is a critical component of seasonal carbon, water and energy cycles in the Earth system. This characteristic is a consequence of plant's adaptive evolutionary processes to a given set of environmental conditions. Changing climate in northern lands (>30°N) alters the state of climatic constraints on plant growth, and therefore, changes in the seasonality and carbon accumulation are anticipated. However, how

This article is protected by copyright. All rights reserved.

Accepted Article

photosynthetic seasonality evolved to its current state, and what role climatic constraints and their variability played in this process and ultimately in carbon cycle is still poorly understood due to its complexity. Here, we take the ‘laws of minimum’ as a basis and introduce a new framework where the timing (Day of Year) of peak photosynthetic activity (DOY_{Pmax}) acts as a proxy for plant’s adaptive state to climatic constraints on its growth. Our analyses confirm that spatial variations in DOY_{Pmax} reflect spatial gradients in climatic constraints as well as seasonal maximum and total productivity. We find a widespread warming-induced advance in DOY_{Pmax} (-1.66 ± 0.30 days decade⁻¹, $P < 0.001$) across northern lands, indicating a spatio-temporal dynamism of climatic constraints to plant growth. We show that the observed changes in DOY_{Pmax} are associated with an increase in total gross primary productivity through enhanced carbon assimilation early in the growing season, which leads to an earlier phase shift in land-atmosphere carbon fluxes and an increase in their amplitude. Such changes are expected to continue in the future based on our analysis of Earth System Model (ESM) projections. Our study provides a simplified, yet realistic framework based on first principles for the complex mechanisms by which various climatic factors constrain plant growth in northern ecosystems.

INTRODUCTION

Warming is generally thought to ease climate constraint on photosynthetic activity of vegetation in northern lands. Indeed, recent growing season studies based on ground observation (Parmesan & Yohe, 2003), eddy covariance (Richardson et al., 2010; Keenan et al., 2014), remote sensing (Xu et al., 2013; Park et al., 2016), and model simulation (Duveneck & Thompson, 2017) have concordantly indicated that the growing season duration for northern terrestrial vegetation has significantly extended over the past decades due to both

Accepted Article

an earlier start and delayed termination. This prolonged growing season over northern land drives a longer carbon assimilation period due to the relaxation of low temperature limits on metabolism, and in turn increased productivity and carbon uptake have been observed (Xu et al., 2013; Forkel et al., 2016). However, longer and warmer growing seasons also promote environmental conditions that favor surface drying, and thus intensified summer droughts, tree mortality, and wildfires have resulted in summer productivity decline (Peng et al., 2011; Barichivich et al., 2014; D'Orangeville et al., 2018). These consequential dynamics are highly variable in space and over time, and indicate a complex interaction of multiple climate constraints on plant growth and its dynamism (Nemani et al., 2003; Garonna et al., 2018; Reich et al., 2018). To accurately project the response of northern vegetation to future climate, we need to better understand how climate-vegetation interaction has evolved to its current state, and what role climatic constraints and their variability played in this process.

Photosynthetic seasonality is an integrated outcome of how plants adapt to seasonal variations in climatic constraints (Chuine & Beaubien, 2001; Jolly et al., 2005; Eagleson, 2005; Garonna et al., 2018), and is thus a critical indicator of vegetation-climate interaction. For instance, gross primary productivity (GPP) tracks the seasonal course of temperature in northern high-latitude ecosystems, while the synchrony between GPP and temperature is gradually lost southwards towards warmer and drier environments (see Figure 1 in Rotenberg & Yakir, 2010). The laws of minimum (Sprengel, 1828; Liebig, 1841; Blackman, 1905) explain these shifts in GPP with respect to varying climatic conditions (Eagleson, 2005). The laws state that although photosynthetic activity is controlled by multiple factors (e.g., radiation, temperature, water availability, etc.), the prevailing rate is set by the most deficient of these factors (Sprengel, 1828; Liebig, 1841; Blackman, 1905). This suggests that the timing (Day of Year) of peak photosynthetic rate ($DOY_{P_{max}}$) during the seasonal course

Accepted Article

corresponds to the period when the primary climatic factor controlling plant growth is least limiting. This simple yet intuitive indicator has an indispensable role not only indicating the timing and magnitude of resource availability (i.e., constraint) but also the capacity of terrestrial ecosystem productivity (Xia et al., 2015; Zhou et al., 2017). Ongoing climate change in the north is expected to alter the state of climatic constraints on plant growth, and therefore, changes in $DOY_{P_{max}}$ and productivity. Previous studies have observed trends toward an earlier peak of the growing season (Buitenwerf et al., 2015; Gonsamo et al., 2018). However, the underlying mechanisms for spatially varying relations between its changes and implications on seasonal total productivity and carbon cycle are still largely unknown.

In this study, we take the ‘laws of minimum’ as a basis and introduce a new framework where the timing of peak photosynthetic activity ($DOY_{P_{max}}$) acts as a proxy for plant’s adaptive state to climatic constraints on its growth. Two basic principles formulate this new framework (Figure 1). First, under non-limiting climatic conditions, $DOY_{P_{max}}$ will show a tendency to coincide with the period of seasonal peak radiation load so as to result in maximum photosynthetic capacity conditions (Eagleson, 2005; Bauerle et al., 2012) (Case 1 in Figure 1). Second, if a climatic factor acts as the primary constraint to photosynthetic activity, $DOY_{P_{max}}$ should shift towards the period in the seasonal course at which that limiting resource is more available (Eagleson, 2005; Rotenberg & Yakir, 2010) (Cases 2–4 in Figure 1). In this framework, the timings of peak GPP ($DOY_{P_{max}}$) and three climatic factors including temperature ($DOY_{T_{max}}$), radiation ($DOY_{R_{max}}$), and water availability ($DOY_{W_{max}}$) serve as key proxies for climate resource availability. We only introduce these three abiotic controls of GPP because it is widely known that they interact to primarily impose complex and varying limitations on vegetation activity (Nemani et al., 2003). Thanks to reduced water losses during the cold season over northern terrestrial ecosystems and thermal inertia, a

This article is protected by copyright. All rights reserved.

sequential order of the timings of peak climatic factors ($DOY_{Wmax} < DOY_{Rmax} < DOY_{Tmax}$) simplifies our framework (Figure S1). In other words, this suggests that positioning of DOY_{Pmax} with respect to DOY_{Rmax} ($\delta DOY_{P,R} = DOY_{Pmax} - DOY_{Rmax}$) can indicate the primary climatic constraint on ecosystems, i.e., water ($\delta DOY_{P,R} < 0$) or temperature ($\delta DOY_{P,R} > 0$). $\delta DOY_{P,T}$ defined as $DOY_{Pmax} - DOY_{Tmax}$ is additionally introduced to subdivide dominant temperature constrained northern ecosystems.

Our primary objectives of this study are two-fold: 1) to examine the proposed framework using independent multiple datasets and understand how northern vegetation seasonality has been characterized; 2) to investigate changes in DOY_{Pmax} and its impact on seasonal total productivity and carbon cycle. To accomplish the objectives, we apply the proposed framework to GPP dynamics from the satellite observed vegetation photosynthetic activity to evaluate its validity and changes in DOY_{Pmax} . Two independent sources of vegetation productivity (tower measured GPP and satellite driven Sun-Induced Fluorescence, SIF) are used to further test the framework. We use the atmospheric CO_2 observations at Point Barrow (71.3° N, 156.6° W) and two state-of-the-art CO_2 inversion estimates to investigate the potential impact of shifting DOY_{Pmax} on terrestrial ecosystem carbon cycle. A set of Earth System Models (ESMs) is additionally introduced to evaluate the reproducibility of the observed DOY_{Pmax} changes and their consequences under historical and future climate scenarios.

MATERIALS AND METHODS

Study area and bioclimatic zones

Only non-agricultural vegetation over north of 30°N is considered in this study to minimize human-induced influence. Three bioclimatic zones including arctic, boreal and temperate regions were used to present outcomes of this study. To discriminate the bioclimatic zones, we combined a terrestrial ecoregion scheme (Olson et al., 2001) of the World Wildlife Fund (WWF) and the Moderate Resolution Imaging Spectroradiometer (MODIS) International Geosphere-Biosphere Programme (IGBP) land cover data (Friedl et al., 2010) (Collection 5.1). We first used MODIS IGBP to keep only non-agricultural vegetation classes (Class 1-10, and 16). Then, based on the WWF's eco-region scheme, tundra and boreal forests/taiga ecoregions were assigned into the arctic and boreal bioclimatic zones, respectively. Temperate broadleaf and mixed forests, temperate coniferous forests, temperate grasslands, savannas, and shrublands were identified as the temperate bioclimatic zone. We further excluded the pixels containing more than 25% of cropland based on the International Institute for Applied Systems Analysis (IIASA) cropland fraction data (Fritz et al., 2015).

Data and methods

Multi-scale GPP and its proxy: satellite and tower measurements

In this study, we mainly used 17-year (2000 to 2016) time series of GPP data from the MODIS aboard NASA's Terra satellite (Running et al., 2015) to examine the framework and to investigate DOY_{Pmax} change in northern lands. The latest version (Collection 6) of MODIS GPP with 8-day temporal composite was spatially aggregated into 0.05 degree grid. Its high temporal frequency is advantageous to capture the seasonal variation of photosynthetic

activity. MODIS GPP is based on a production efficiency model that uses the product of the absorbed photosynthetically active radiation by vegetation and a light use efficiency factor. The quality of MODIS GPP data sets has been comprehensively evaluated against multiple eddy-covariance tower measurements of GPP and through inter-comparisons with other GPP products (Zhao et al., 2005; Heinsch et al., 2006).

We additionally introduced satellite-driven SIF and eddy-covariance based GPP data to verify our framework and results from MODIS GPP. The SIF is retrieved near the $\lambda = 740$ nm far-red peak in chlorophyll fluorescence emission from the Global Ozone Monitoring Experiment-2 (GOME-2) instrument onboard Eumetsat's MetOp-A satellite. The monthly SIF record (version 27, level 3) covering 2007 to 2016 was used in this study (Joiner et al., 2016). SIF is an electromagnetic emission in the 650-800 nm range originating from plant photosynthetic machinery, and it is theoretically linearly correlated with the electron transport rate of photosynthetic activity (Zhang et al., 2014).

The eddy-covariance tower measurements from the FLUXNET2015 database (tier 1, Pastorello et al., 2017) were used in this study. FLUXNET is a global network of micrometeorological tower sites that use eddy covariance methods to measure the exchanges of carbon, water, and energy between terrestrial ecosystems and the atmosphere (Baldocchi et al., 2001). We used GPP estimates based on the flux partitioning approach proposed by Lasslop et al. (2010). A total of 92 sites (those with more than 3 site-year measurements) were selected for the evaluation of our $DOY_{P_{max}}$ framework spanning a large climatic and biome gradient (Figure S2a).

Multi-scale climate data

We used daily climate datasets provided by Global Modeling and Assimilation Office (GMAO) Reanalysis of NASA (Gelaro et al., 2017). The current version of GMAO is an hourly time step dataset generated by Goddard Earth Observing System-5 (GEOS-5) data assimilation system. We aggregated the native hourly data into the daily scale to retrieve pixel-wise phases of climate variables. Surface air temperature and down-welling photosynthetically active radiation were employed in this analysis. Daily climate datasets were used to characterize $DOY_{T_{max}}$ and $DOY_{R_{max}}$. We also obtained potential evapotranspiration (PET) and actual evapotranspiration (AET) to quantify water availability on plant growth by calculating a ratio of AET to PET (RAP) (Prentice et al., 1992). Both AET and PET were obtained by Global Land Data Assimilation Systems (GLDAS, Version 2.1) (Rodell et al., 2004). We characterized summer climate using mean temperature and RAP during June–August for investigating how $DOY_{P_{max}}$ positioning varies as functions of climate constraints, i.e., temperature and water availability. For the tower measured GPP, the ancillary microclimate datasets including air temperature and incoming radiation (Photosynthetic photon flux density, PPFD) simultaneously measured with GPP were additionally obtained.

Earth System Model simulated historical and future GPP

We also introduced a set of the most recent climate-carbon simulations of ESMs contributing to the fifth phase of the Coupled Model Intercomparison Project, CMIP5 (Taylor et al., 2012). Seven ESMs, which are available at CMIP5 archive, were used in this study: NorESM1-M, MIROC-ESM, CanESM2, HadGEM2-ES, IPSL-CM5A-MR, MPI-ESM-MR and CCSM4. The datasets provided monthly GPP output (1980 to 2099) for simulations of

both Historical and Representative Concentration Pathway (RCP) 4.5 (Thomson et al., 2011). Data from the Historical and RCP4.5 scenario periods were combined to generate continuous variable fields from 1980 to 2099. All model outputs were processed at the native spatial resolutions and aggregated into regional scales (i.e., arctic, boreal, and temperate regions) for trend and correlation estimates.

Timings of peak seasonal photosynthetic activity and climate

We extracted three metrics indicating a maximal state of seasonal photosynthetic activity ($DOY_{P_{max}}$), radiation ($DOY_{R_{max}}$), and temperature ($DOY_{T_{max}}$) at two different scales: site and regional scale. For both scales, to reduce noise and maintain a distinct seasonal feature of GPP (or SIF) and climate datasets, the singular spectrum analysis was first implemented at yearly basis (Vautard et al., 1992). The singular spectrum analysis is a nonparametric approach that does not need a priori specification of models of time series, thus it is data-adaptive. It first decomposes a time series into oscillatory components and noises according to the singular value decomposition, thereafter reconstructs specific components (i.e., seasonal signal) from the original time series. This non-parametric approach has been widely used to reconstruct the time series of GPP and other environmental variables by reducing their noise components (Keenan et al., 2014; Zhou et al., 2017). Time series of GPP and meteorological datasets were used to retrieve $DOY_{P_{max}}$, $DOY_{R_{max}}$, and $DOY_{T_{max}}$ on a yearly basis. Note that multi-year averaged daily GPP, radiation, and temperature time series were used for FLUXNET retrievals. For the case of monthly data (SIF and CMIP5 GPP), we assigned middle of the month as the day of the year for each month and then implemented the same procedures used in MODIS and FLUXNET. Finally, $\delta DOY_{P,R}$ (i.e., $DOY_{P_{max}} - DOY_{R_{max}}$) and $\delta DOY_{P,T}$ (i.e., $DOY_{P_{max}} - DOY_{T_{max}}$) were also calculated. We additionally

retrieved pixel-wise growing season length from MODIS GPP by applying a fixed threshold, i.e., 10% of the multi-year average maximum GPP (Zhou et al., 2017).

Atmospheric CO₂ concentration and fluxes: zero-crossing date and seasonal amplitude

Daily atmospheric CO₂ concentration at Point Barrow (71.3° N, 156.6° W) was obtained from the in situ measurement dataset provided by the National Oceanic and Atmospheric Administration / Earth System Research Laboratory (NOAA / ESRL). The spring downward CO₂ zero-crossing date (DOY_{Zero-Crossing}) was extracted by following the approach described in Piao et al. (2008). We first detrended the interannual trend in the atmospheric CO₂ concentration with a quadratic polynomial curve, four harmonics in the seasonal function, and time-filtered residuals. We then used the harmonics plus the residuals (detrended CO₂ seasonal cycle) to define the downward CO₂ DOY_{Zero-Crossing} as the day on which the detrended curve crossed the zero line from positive to negative. All aforementioned processes were achieved by the use of the standard package CCGCRV from NOAA/ESRL (Thoning et al., 1989). We used DOY_{Zero-Crossing} as an indicator of proximal DOY_{Pmax} for three reasons, although DOY_{Zero-Crossing} is not an accurate term of peak photosynthesis timing. First, seasonal trajectory of GPP strongly governs changes in net biome productivity seasonality and its trend (Ito et al., 2016; Forkel et al., 2016). Second, DOY_{Zero-Crossing} can be determined more accurately and it is roughly corresponding to the time of maximum carbon uptake by the biosphere (Ito et al., 2016). Third, a relative change in the phase of the cycle identified at one point (e.g. DOY_{Zero-Crossing}) will be matched by relative phase changes at all other points since the shape of the seasonal cycle does not change significantly (Barichivich et al., 2012). We further extracted the seasonal cycle amplitude (SCA) because its changes reflect vegetation GPP driven changes in net carbon uptake (Forkel et al., 2016).

We additionally used two gridded carbon fluxes from atmospheric CO₂ inversion products: the Copernicus Atmosphere Monitoring Service (Chevallier et al., 2010) (CAMS, version v15r2, 1979-2015) and the Jena CarboScope (Rödenbeck et al., 2003) (JENA, version s81_v3.8, 1981-2015). Atmospheric CO₂ inversions estimate net carbon exchange fluxes between surface and atmosphere by utilizing CO₂ concentrations at measurement sites, combined with an atmospheric transport model and prior information on fossil fuel carbon emissions and carbon exchange between the atmosphere and land (and ocean). We used daily mean net flux estimates on a spatial resolution of 3.75° latitude and 5° longitude (JENA) and 1.875° latitude and 3.75° longitude (CAMS) over the vegetated land surface. Both products were firstly aggregated into regional scales then DOY_{Zero-Crossing} and SCA of carbon fluxes were respectively extracted. Note that the flux amplitude is indirectly related to the amplitude in the atmospheric CO₂ concentration, as the atmospheric concentration is roughly the integral of the fluxes (Welp et al., 2016).

Analytical approach

Based on the extracted MODIS DOY_{Pmax}, we first tested the validity of framework by relating it to summer climate conditions (i.e., temperature and water availability). The first principle we formulated for the framework justifies using summer season as a period when the primary climate constraint dictates vegetation photosynthetic seasonality, and therefore, DOY_{Pmax}. Both seasonal total (GPP_{Total}) and maximum GPP (GPP_{Pmax}) were calculated to investigate the spatial and temporal relations between DOY_{Pmax} and vegetation productivity. In order to capture the seasonal distribution of GPP with a simple metric, we evaluated the ratio (GPP_{Ratio}) of total GPP during the first half (January 1st to the long-term mean DOY_{Pmax}) to that of the whole year. Additionally, the length of growing season together with GPP_{Pmax}

was considered to explain the observed pattern between $DOY_{P_{max}}$ and GPP_{Total} (e.g., Xia et al., 2015). All explored relationships were explained as functions of $\delta DOY_{P,R}$ and $\delta DOY_{P,T}$. Independent eddy-covariance tower GPP and GOME-2 SIF based retrievals were used for further testing of the framework. Note that we limited the use of these independent data only for verifying the framework and not the change analysis because of limited temporal frequency and coverage of the data.

For the time series analysis, all trends in time series were computed as the slope of linear trends based on ordinary least squares regression. The significance of the trend was computed by using the non-parametric Mann-Kendall trend test. The standard error of the trend slope is also reported. We estimated the decadal trend based on the 5-year moving average approach to reduce the potential impact of first, last and outlier points. The Kendall's rank correlation coefficient (r) was used to measure the ordinal association between given two quantities. To understand how warming-induced $DOY_{P_{max}}$ shift has characterized northern land vegetation productivity, we investigated changes in temperature, $DOY_{P_{max}}$, GPP_{Total} , and GPP_{Ratio} . This analysis was applied to both MODIS and ESMs based retrievals. A trend in $DOY_{zero-crossing}$ of three CO_2 data was respectively computed and correlation analysis between annual variations in $DOY_{zero-crossing}$ and SCA was performed.

RESULTS

Spatial pattern of MODIS $DOY_{P_{max}}$ and its determinants

A distinct spatial gradient exists in $DOY_{P_{max}}$ and in its positioning with respect to the seasonal course of radiation and temperature (Figures 2a and Figure S2a,b). Overall,

Accepted Article

DOY_{Pmax} in arctic ecosystems is more closely aligned with DOY_{Tmax} ($\delta\text{DOY}_{P,T} = -9.3 \pm 5.5$ days, mean \pm 1 s.d.) than DOY_{Rmax} ($\delta\text{DOY}_{P,R} = 29.1 \pm 8.5$ days), while in the boreal ecosystems it shows a much closer alignment with peak radiation levels ($\delta\text{DOY}_{P,T} = -13.3 \pm 5.4$ days, $\delta\text{DOY}_{P,R} = 12.9 \pm 10.5$ days). In the temperate regions, $\delta\text{DOY}_{P,R}$ is negative (-9.5 ± 27.0 days), i.e., DOY_{Pmax} precedes DOY_{Rmax}. Temperature and water availability (i.e., RAP) limiting photosynthetic activity elucidate the observed regional variations in DOY_{Pmax} positioning. Every 1 °C increase in temperature results in a $\delta\text{DOY}_{P,R}$ change of -5.7 ± 0.1 days (slope \pm SE, Figure 2b). In regions with negative $\delta\text{DOY}_{P,R}$, every 1% decrease in water availability results in a $\delta\text{DOY}_{P,R}$ change of -1.8 ± 0.1 days (Figure 2c). These results follow the two tenets of our framework, as outlined earlier complying with the laws of minimum (Sprengel, 1828; Liebig, 1841; Blackman, 1905). This suggests that the use of DOY_{Pmax} and its positioning in relation to DOY_{Rmax} and DOY_{Tmax} represents a feasible approach to assess plant's adaptive state to climatic constraints.

Climate constraints, MODIS DOY_{Pmax} and seasonal vegetation productivity

Emerging climatic constraints to plant growth are directly linked to changes in both GPP_{Total} (Figure 2d) and GPP_{Pmax} (Figure S2c). Regions with large GPP_{Pmax} are associated with tight synchrony between DOY_{Pmax} and DOY_{Rmax}, i.e., both energy and water accessibility are least limiting (Bauerle et al., 2012). Ecosystems under either temperature- ($\delta\text{DOY}_{P,R} > 0$) or water-limited ($\delta\text{DOY}_{P,R} < 0$) environments show lower photosynthetic capacity by complying the general idea of climatic constraints to plant growth. Such interaction limiting photosynthetic activity is also tightly associated with growing season duration (Figure S2d). It is interesting to note that in areas with the largest GPP_{Total} ($\sim 1.07 \text{ kg C m}^{-2}$), DOY_{Pmax} slightly precedes DOY_{Rmax} ($\delta\text{DOY}_{P,R} \approx -7$ days) because of a joint control by growing season length and GPP_{Pmax} (Xia et al., 2015). The longest growing season duration (~ 6.5 months) is found

when $\delta\text{DOY}_{P,R}$ is approximately equal to -17 days. This is known as ‘phenological trade-off’, i.e., a longer growing season imposed by warmer environment may result in a higher $\text{GPP}_{\text{Total}}$, but warmer and drier summers may suppress GPP_{Pmax} , potentially offsetting the increased amount of $\text{GPP}_{\text{Total}}$ (Duveneck & Thompson, 2017).

Confirmed patterns from two independent data: SIF and Eddy-Covariance tower GPP

Flux tower-measured GPP data from the eddy-covariance network and GOME-2 SIF confirm the above patterns observed in MODIS GPP products, thus lending further support for the proposed DOY_{Pmax} framework (Figures 3 and Figure S3).

Changes in MODIS DOY_{Pmax} during last 17 years

Trend analyses reveal a widespread shift in MODIS DOY_{Pmax} towards earlier in the growing season dominating across 60.6 % of the northern vegetated area during last 17 years, and 32.8 % of the area showing a significant negative trend ($P < 0.1$, Figure 4). These changes are seen across all three bioclimatic zones, i.e., 31.9 %, 38.7 % and 26.8 % of the arctic, boreal and temperate regions, respectively. At a hemispheric scale, we detected a significant trend towards an earlier peak photosynthetic rate of -1.66 ± 0.30 days decade⁻¹ (slope \pm s.e., $P < 0.001$) (Figure 5a), with regionally varying degree of advancing trends: a steeper change in the boreal region (-2.46 ± 0.47 days decade⁻¹, $P < 0.001$) relative to the temperate (-1.07 ± 0.26 days decade⁻¹, $P < 0.001$) and arctic regions (-1.09 ± 0.29 days decade⁻¹, $P < 0.001$). These changes are mostly associated with warming in the lands north of 30°N (Figure 4b and Figure 5b). The sensitivity of DOY_{Pmax} to warming was detected to be greater in the temperate (-4.27 ± 1.50 days °C⁻¹, $P < 0.001$) than in the arctic (-3.88 ± 1.29 days °C⁻¹, $P < 0.001$) and boreal (-3.91 ± 1.02 days °C⁻¹, $P < 0.001$) regions. Note that regionally varying

warming rates (TE < AR < BO) lead to a different order of trend and sensitivity estimates. These changes in $DOY_{P_{max}}$ are interpreted as shifts in $\delta DOY_{P,R}$ across the arctic (-1.98 ± 7.30 days, mean \pm SD, t -test, $P < 0.001$), boreal (-3.21 ± 5.83 days, $P < 0.001$) and temperate (-1.28 ± 12.76 days, $P < 0.001$) regions (Figure S4a,b). We find that the observed shift in $DOY_{P_{max}}$ is mainly responsible for the changes in $\delta DOY_{P,R}$ (and $\delta DOY_{P,T}$) because of relatively stable $DOY_{R_{max}}$ and $DOY_{T_{max}}$ changes (Figure S4 and Table S1). According to the principles in our framework, the shifts resulting a newly established photosynthetic seasonality with respect to seasonal climate factors imply changes in vegetation response to varying climatic constraints, i.e., reduced relative importance of thermal constraint in the arctic and boreal vegetation while enhanced role of water availability in the temperate regions (Garonna et al., 2018; Piao et al., 2017; Fu et al., 2015; Allen et al., 2010) (Figures 2b,c and 5a). Note that some regions transitioning from positive to negative $\delta DOY_{P,R}$ might experience a critical tipping point where the ecosystems moves from temperature- towards water-limited ecosystems (Figure S5).

Implications of changing MODIS $DOY_{P_{max}}$ on seasonal vegetation productivity

The changes in $DOY_{P_{max}}$ have regionally varying impacts on GPP_{Total} . An ‘earlier peak–larger productivity’ pattern is dominant over the arctic (-0.004 ± 0.002 kg C m⁻² day⁻¹, slope \pm s.e., $P < 0.05$) and boreal (-0.006 ± 0.002 kg C m⁻² day⁻¹, $P < 0.05$) regions under a warming climate (Figure 5c). The framework proposed earlier informs that more favorable thermal conditions enable vegetation to increase its synchrony with seasonality in incoming radiation, with the seasonal course of photosynthetic activity tending toward the peak of radiation. Widely reported growing season extension (likely inferred from $DOY_{P_{max}}$ shift, Figure S2d) partly explains such ‘earlier peak–larger productivity’ relation across the arctic and boreal regions (Xu et al., 2013; Park et al., 2016). Warmer temperatures might also

Accepted Article

enhance access to key nutrients (e.g., nitrogen), thus stimulating photosynthetic rates over the course of the entire growing season (Natali et al., 2012). A weaker ‘earlier peak–less productivity’ pattern in the temperate regions emerges due to complex climate-vegetation interactions (Figure 5c). Here, warmer conditions without moisture-stress result in an earlier DOY_{Pmax} and larger GPP_{Pmax} and $\text{GPP}_{\text{Total}}$. In other parts, where moisture stress is stronger, a significant decline in both GPP_{Pmax} and $\text{GPP}_{\text{Total}}$ is seen despite earlier DOY_{Pmax} (e.g., southwestern Eurasia) (Angert et al., 2005). In order to capture the seasonal distribution of GPP with a simple metric we evaluated the ratio ($\text{GPP}_{\text{Ratio}}$) of total GPP during the first half (January 1st to the long-term mean DOY_{Pmax}) to that of the whole year. We find that DOY_{Pmax} occurring one day earlier in the season increases $\text{GPP}_{\text{Ratio}}$ by 0.28 ± 0.07 (temperate, slope \pm SE, $P < 0.001$) to 0.58 ± 0.08 % (boreal, $P < 0.001$), clearly indicating an advance in gross carbon assimilation activity (Figure 5d) (Duvencek & Thompson, 2017). This is an important indicator, as the photosynthetic activity is tightly linked to the atmosphere via carbon, water and energy cycles. Thus, phase shifts in carbon, water and energy cycles could be anticipated (Richardson et al., 2013).

Changes in phase and amplitude of CO₂ seasonal cycle

We found that earlier peak photosynthesis and more carbon assimilation in the early part of the growing season altered the seasonal course of atmospheric CO₂ concentration. We used CO₂ observations from Point Barrow and two state-of-the-art CO₂ inversion datasets (i.e., CAMS and JENA). The springtime downward CO₂ zero-crossing date ($\text{DOY}_{\text{Zero-Crossing}}$) shows trends towards earlier downward $\text{DOY}_{\text{Zero-Crossing}}$ in the three CO₂ datasets (Figure 6a). The phase of atmospheric CO₂ at Point Barrow has advanced by 1.84 ± 0.20 days decade⁻¹ (slope \pm SE, $P < 0.001$) since 1972. We also observe advancing trends but steeper changes in both CAMS (-2.42 ± 0.21 days decade⁻¹, $P < 0.001$) and JENA (-3.26 ± 0.21 days decade⁻¹, $P < 0.001$). This article is protected by copyright. All rights reserved.

P < 0.001). This shift corroborates the advancing $DOY_{P_{max}}$ of gross photosynthetic activity observed from space and shows the potential implications of enhanced gross carbon assimilation in the early growing season (i.e., increased GPP_{Ratio}) (Barichivich et al., 2012; Randerson et al., 1999) (Figure 5a,d). Furthermore, like as what we observed in the analysis of $DOY_{P_{max}}$ and GPP_{Total} (Figure 5c), SCA of three CO_2 data is negatively associated with $DOY_{Zero-Crossing}$ (Figure 6b). These phase shifts in the CO_2 data and their association with the enhanced seasonal amplitudes are in accordance with several observations (Barichivich et al., 2012; Randerson et al., 1999; Graven et al., 2013) and modeling studies (Duveneck & Thompson, 2017; Zhao & Zeng, 2014) suggesting enhanced peak photosynthetic activity and its advancing shift.

Changes in ESMS simulated vegetation productivity and $DOY_{P_{max}}$

We lastly ask whether state-of-the-art terrestrial biosphere models can reproduce the observed $DOY_{P_{max}}$ changes and their consequences under historical and future climate scenarios (Figure 7). The ESMS project an advancing $DOY_{P_{max}}$ across all northern bioclimatic zones for the period 1980 to 2030. We see a pattern of regional $DOY_{P_{max}}$ trends from ESMS analogous to satellite observations, i.e. a strong trend for shifting to earlier in the season over the boreal (-0.94 ± 0.67 days decade⁻¹, mean \pm 1 s.d. across all ESMS), arctic (-0.86 ± 0.71 days decade⁻¹) and temperate (-0.58 ± 0.61 days decade⁻¹) regions. All models show a tightly linked negative relation between $DOY_{P_{max}}$ and GPP_{Total} , revealing the ‘earlier peak-larger productivity’ tendency as in current satellite observations. Particularly, temperature-constrained arctic and boreal regions have a tighter linkage between $DOY_{P_{max}}$ and GPP_{Total} than the warmer temperate regions. The shift in $DOY_{P_{max}}$ also increases the GPP_{Ratio} , indicating more carbon assimilation in the early part of the growing season than in the later period (Duveneck & Thompson, 2017; Zhao & Zeng, 2014). The pace of future

This article is protected by copyright. All rights reserved.

(2050 – 2100) DOY_{Pmax} shift and its contribution to productivity is projected to continue, but to be slower and weaker than at present.

DISCUSSION

Our analyses from long-term satellite records and ESMs reveal a widespread shift in DOY_{Pmax} towards earlier in the growing season. The changes are associated with divergent consequences on $\text{GPP}_{\text{Total}}$ depending on different states of climate constraints on plant growth. For high latitude arctic ecosystems, the advancement in DOY_{Pmax} likely continues in a warmer future climate as seen in the ESM simulations. Our framework translates the change into a continuous relaxation of temperature limit on arctic vegetation photosynthetic activity. A recent remote sensing based study supports our study by identifying a 16.4% decline in the area of vegetated land that is limited by temperature (Keenan & Riley, 2018). Yet, our framework suggests a reduction in the relative importance of temperature control on plant photosynthetic activity rather than a transitional state where other climate constraints primarily govern the ecosystem (Figure S4a). Indeed, long-term ground based studies in the Arctic tundra have shown that temperature is a primary driver of shrub growth and its expansion in arctic environment, while soil moisture controls the sensitivity of growth response to warming (Myers-Smith et al., 2015).

Some of boreal ecosystems (northwest Russia and south Fennoscandia, south and southeast Canada) show a transition from positive to negative $\delta\text{DOY}_{\text{P,R}}$ during last two decades (Figure S5). This transition does not necessarily signify a decline of $\text{GPP}_{\text{Total}}$ because of the “phenological tradeoff” mechanism (Figure S2d). However, it is critical to monitor these ecosystems continuously because our framework suggests that there may be a tipping point

This article is protected by copyright. All rights reserved.

where they move from temperature- towards water-limited ecosystems. That is, continuous warming and drying conditions may exacerbate moisture stress, and therefore, productivity reduction in these ecosystems. Interestingly, a recent tree-ring based study revealed that while 2 °C of warming may increase overall forest productivity, additional warming could reverse this trend and lead to substantial moisture stress (D'Orangeville et al., 2018). Also, multiple warming experiments confirm the dynamism of climate constraints on plant growth in the southern boreal forest and highlight the vulnerability of the ecosystem to excess warming and drying (e.g., Reich et al., 2018).

Warmer and drier conditions over temperate vegetation, where negative $\delta\text{DOY}_{P,R}$ is dominant, generally result in a decrease of plant growth. Widespread increase of tree mortality of this susceptible ecosystem to worsening moisture stress has been reported (Allen et al., 2010). Most epidemic climate-induced tree mortality events occurs over the regions where water availability is the primary climate constraint on photosynthetic activity (i.e., $\delta\text{DOY}_{P,R} < 0$, see Figure S5). It agrees with the 'earlier peak–less productivity' pattern in warmer temperate vegetation from MODIS data. However, the relation was not reproduced by the ESMs. The models projected that warming-induced earlier peak photosynthesis leads to an enhanced seasonal total productivity (Figure 7a). Recent studies have shown that current terrestrial carbon-cycle models substantially overestimate (underestimate) positive (negative) effects associated with warming (Buermann et al., 2018). It is possibly because these models inadequately capture the effects of the seasonal build-up of water stress on seasonal vegetation growth.

Our analyses of $DOY_{\text{zero-crossing}}$ and SCA confirm the advancing and enhancing CO_2 seasonal cycle in northern lands (Barichivich et al., 2012; Graven et al., 2013; Forkel et al., 2016). An additional remark made here for ongoing changes in biosphere-atmosphere interaction is an asymmetric enhancement of terrestrial photosynthetic activity. We find a widespread warming-induced DOY_{Pmax} advancement and GPP_{Total} increase across northern lands, and these changes possibly play a role in ongoing shift and amplified atmospheric CO_2 seasonal cycle. This is because peak photosynthesis rate explains about 78% of the variation of seasonal total productivity and only 21% can be explained by growing season changes (Xia et al., 2015). Our results confirm that a larger beneficial carbon uptake from an extended growing season is dominated by the later part of spring, when more fully developed leaf area with more favorable light and temperature is available for photosynthetic activity (Keenan et al., 2014). Together with these earlier studies, our findings suggest that an intra-seasonal scale may provide a possible but overlooked mechanism for the changes in atmospheric CO_2 seasonal cycle. Furthermore, the observed shift in the relative importance of climate constraints on plant growth may be a possible mechanism for the recently reported weakening temperature controls on spring carbon uptake across northern lands (Piao et al., 2017).

Furthermore, our framework also gives insight into the changes in growing season duration and its implication on carbon cycle. As described in Figure 1, thermal inertia induced decoupling of radiation and temperature characterizes a unique seasonal climate environment to local vegetation. For temperature-constrained ecosystems (see Case-2 in Figure 1), DOY_{Tmax} -ward DOY_{Pmax} positioning leads to strong temperature dependence in spring photosynthesis while light availability emerges as an important controller in autumnal activity (Garonna et al., 2018). This intrinsic physical environment indicates contrasting

This article is protected by copyright. All rights reserved.

Accepted Article

responses of photosynthetic activity to spring versus autumn warming. In this cold environment, spring warming generally stimulates carbon uptake by extending onset of growing season (Pulliainen et al., 2017). In contrast, autumnal growing season extension and its photosynthetic carbon gain will be strongly limited by radiation (Bauerle et al., 2012). Multiple studies have reported that the increase of autumn temperature results in net carbon loss indicating more respiratory loss than photosynthetic gain in northern lands (Piao et al., 2008; Commane et al. 2017). These contrasting seasonal responses also partially explain the observed and projected asymmetric enhancement of photosynthetic activity and carbon cycles in northern lands. However, further studies will be required to identify which case the autumn growing season extension can lead to increased photosynthesis sufficient to balance the higher respiration carbon loss.

Most of ESMs as well as MODIS GPP estimate used in this study do not include photosynthetic temperature acclimation process. This physiological adjustment is commonly observed as a shift in the optimum temperature for carbon assimilation rate by modulating local plant's metabolism (Yamori et al., 2014). We expect that taking the photosynthetic thermal acclimation likely lead to a slightly closer alignment between $DOY_{P_{max}}$ and $DOY_{R_{max}}$ than the one without the process. It also may reduce the observed $DOY_{P_{max}}$ sensitivity to warming (Smith et al., 2016). Nevertheless, we believe that the proposed $DOY_{P_{max}}$ framework and its changes are valid because of multiple evidence from independent datasets in this work (Figures 3 and Figure S3) and previous studies (Rotenberg & Yakir, 2010; Buitenwerf et al., 2015; Gonsamo et al., 2018). Interestingly, dendrometer based intra-annual tree growth studies also support our framework (e.g., Rossi et al., 2006). Ongoing efforts for advancements in modeling communities (Rogers et al., 2017) will help to deploy temperature

acclimation modules in ESMs and thus better understandings on seasonal photosynthesis and DOY_{Pmax} changes are expected.

In summary, our results highlight a significant shift in terrestrial photosynthetic activity north of 30°N , implying a constantly adapting state of climatic constraints on plant growth. A consensus of multiple Earth observations and ESMs on this change imbues confidence in our findings. This is a critical development because the shifts in peak photosynthesis may cause cascading perturbations in Earth system components that include carbon, water and energy balances (Richardson et al., 2013), as well as ecological interactions (Walther, 2010). The framework proposed here is one of the first attempts to introduce the time of peak photosynthesis as an indicator of a plant's adaptive state to climatic constraints, and provides a simplified yet realistic framework for the complex mechanisms by which various climatic factors constrain plant growth.

ACKNOWLEDGEMENTS

This work was funded by NASA Earth Science Directorate (grants NNX16AO34H, NNX14AP80A and NNX14AI71G) and the Research Council of Norway (grants 227064 and 270992). A Natural Environment Research Council Independent Research Fellowship (NE/L011859/1) funded M.M.-F.'s contribution.

AUTHOR CONTRIBUTIONS

TP and RBM designed the research; TP performed analysis and wrote the draft; and all the authors contributed to the interpretation of the results and the writing of the paper.

REFERENCES

- Allen, C. D., Macalady, A. K., Chenchouni, H., Bachelet, D., McDowell, N., Vennetier, M., . . . Hogg, E. T. (2010). A global overview of drought and heat-induced tree mortality reveals emerging climate change risks for forests. *Forest Ecology and Management*, 259(4), 660-684.
- Angert, A., Biraud, S., Bonfils, C., Henning, C., Buermann, W., Pinzon, J., . . . Fung, I. (2005). Drier summers cancel out the CO₂ uptake enhancement induced by warmer springs. *Proceedings of the National Academy of Sciences of the United States of America*, 102(31), 10823-10827.
- Baldocchi, D., Falge, E., Gu, L., Olson, R., Hollinger, D., Running, S., . . . Evans, R. (2001). FLUXNET: A new tool to study the temporal and spatial variability of ecosystem-scale carbon dioxide, water vapor, and energy flux densities. *Bulletin of the American Meteorological Society*, 82(11), 2415-2434.
- Barichivich, J., Briffa, K. R., Osborn, T. J., Melvin, T. M., & Caesar, J. (2012). Thermal growing season and timing of biospheric carbon uptake across the Northern Hemisphere. *Global Biogeochemical Cycles*, 26(4).
- Barichivich, J., Briffa, K. R., Myneni, R., Schrier, G. V. D., Dorigo, W., Tucker, C. J., ... & Melvin, T. M. (2014). Temperature and snow-mediated moisture controls of summer

photosynthetic activity in northern terrestrial ecosystems between 1982 and 2011. *Remote Sensing*, 6(2), 1390-1431.

Bauerle, W. L., Oren, R., Way, D. A., Qian, S. S., Stoy, P. C., Thornton, P. E., . . . Reynolds, R. F. (2012). Photoperiodic regulation of the seasonal pattern of photosynthetic capacity and the implications for carbon cycling. *Proceedings of the National Academy of Sciences*, 109(22), 8612-8617.

Blackman, F. F. (1905). Optima and limiting factors. *Annals of botany*, 19(74), 281-295.

Buermann, W., Forkel, M., O'Sullivan, M., Sitch, S., Friedlingstein, P., Haverd, V., ... & Lombardozzi, D. (2018). Widespread seasonal compensation effects of spring warming on northern plant productivity. *Nature*, 562(7725), 110.

Buitenwerf, R., Rose, L., & Higgins, S. I. (2015). Three decades of multi-dimensional change in global leaf phenology. *Nature Climate Change*, 5(4), 364.

Chevallier, F., Ciais, P., Conway, T., Aalto, T., Anderson, B., Bousquet, P., . . . Fröhlich, M. (2010). CO₂ surface fluxes at grid point scale estimated from a global 21 year reanalysis of atmospheric measurements. *Journal of Geophysical Research: Atmospheres*, 115(D21).

Chuine, I., & Beaubien, E. G. (2001). Phenology is a major determinant of tree species range. *Ecology Letters*, 4(5), 500-510.

Commane, R., Lindaas, J., Benmergui, J., Luus, K.A., Chang, R.Y.W., Daube, B.C., . . . Miller, S.M. (2017). Carbon dioxide sources from Alaska driven by increasing early winter respiration from Arctic tundra. *Proceedings of the National Academy of Sciences*, 114(21), 5361-5366.

- Duveneck, M. J., & Thompson, J. R. (2017). Climate change imposes phenological trade-offs on forest net primary productivity. *Journal of Geophysical Research: Biogeosciences*, 122(9), 2298-2313.
- D'Orangeville, L., Houle, D., Duchesne, L., Phillips, R. P., Bergeron, Y., & Kneeshaw, D. (2018). Beneficial effects of climate warming on boreal tree growth may be transitory. *Nature communications*, 9(1), 3213.
- Eagleson, P. S. (2005). *Ecohydrology: Darwinian expression of vegetation form and function*. Cambridge University Press.
- Forkel, M., Carvalhais, N., Rödenbeck, C., Keeling, R., Heimann, M., Thonicke, K., . . . Reichstein, M. (2016). Enhanced seasonal CO₂ exchange caused by amplified plant productivity in northern ecosystems. *Science*, 351(6274), 696-699.
- Friedl, M. A., Sulla-Menashe, D., Tan, B., Schneider, A., Ramankutty, N., Sibley, A., & Huang, X. (2010). MODIS Collection 5 global land cover: Algorithm refinements and characterization of new datasets. *Remote Sensing of Environment*, 114(1), 168-182.
- Fritz, S., See, L., McCallum, I., You, L., Bun, A., Moltchanova, E., . . . Perger, C. (2015). Mapping global cropland and field size. *Global Change Biology*, 21(5), 1980-1992.
- Fu, Y. H., Zhao, H., Piao, S., Peaucelle, M., Peng, S., Zhou, G., ... & Song, Y. (2015). Declining global warming effects on the phenology of spring leaf unfolding. *Nature*, 526(7571), 104.
- Garonna, I., de Jong, R., Stöckli, R., Schmid, B., Schenkel, D., Schimel, D., & Schaepman, M. E. (2018). Shifting relative importance of climatic constraints on land surface phenology. *Environmental Research Letters*, 13(2), 024025.

- Gelaro, R., McCarty, W., Suárez, M. J., Todling, R., Molod, A., Takacs, L., ... & Wargan, K. (2017). The modern-era retrospective analysis for research and applications, version 2 (MERRA-2). *Journal of Climate*, 30(14), 5419-5454.
- Gonsamo, A., Chen, J. M., & Ooi, Y. W. (2018). Peak season plant activity shift towards spring is reflected by increasing carbon uptake by extratropical ecosystems. *Global change biology*, 24(5), 2117-2128.
- Graven, H. D., Keeling, R. F., Piper, S. C., Patra, P. K., Stephens, B. B., Wofsy, S. C., ... & Daube, B. C. (2013). Enhanced seasonal exchange of CO₂ by northern ecosystems since 1960. *Science*, 1239207.
- Heinsch, F. A., Zhao, M., Running, S. W., Kimball, J. S., Nemani, R. R., Davis, K. J., . . . Ricciuto, D. M. (2006). Evaluation of remote sensing based terrestrial productivity from MODIS using regional tower eddy flux network observations. *IEEE Transactions on Geoscience and Remote Sensing*, 44(7), 1908-1925.
- Ito, A., Inatomi, M., Huntzinger, D. N., Schwalm, C., Michalak, A. M., Cook, R., . . . Post, W. M. (2016). Decadal trends in the seasonal-cycle amplitude of terrestrial CO₂ exchange resulting from the ensemble of terrestrial biosphere models. *Tellus B: Chemical and Physical Meteorology*, 68(1), 28968.
- Joiner, J., Yoshida, Y., Guanter, L., & Middleton, E. M. (2016). New methods for the retrieval of chlorophyll red fluorescence from hyperspectral satellite instruments: simulations and application to GOME-2 and SCIAMACHY. *Atmospheric Measurement Techniques*, 9(8).
- Jolly, W. M., Nemani, R., & Running, S. W. (2005). A generalized, bioclimatic index to predict foliar phenology in response to climate. *Global Change Biology*, 11(4), 619-632.

- Keenan, T. F., Gray, J., Friedl, M. A., Toomey, M., Bohrer, G., Hollinger, D. Y., . . . Wing, I. S. (2014). Net carbon uptake has increased through warming-induced changes in temperate forest phenology. *Nature Climate Change*, 4(7), 598-604.
- Keenan, T., & Riley, W. (2018). Greening of the land surface in the world's cold regions consistent with recent warming. *Nature Climate Change*, 8(9), 825.
- Lasslop, G., Reichstein, M., Papale, D., Richardson, A. D., Arneeth, A., Barr, A., . . . Wohlfahrt, G. (2010). Separation of net ecosystem exchange into assimilation and respiration using a light response curve approach: critical issues and global evaluation. *Global Change Biology*, 16(1), 187-208.
- Liebig, J. (1841). *Organic chemistry in its applications to agriculture and physiology*. J. Owen.
- Myers-Smith, I. H., Elmendorf, S. C., Beck, P. S., Wilkening, M., Hallinger, M., Blok, D., ... & Speed, J. D. (2015). Climate sensitivity of shrub growth across the tundra biome. *Nature Climate Change*, 5(9), 887.
- Natali, S. M., Schuur, E. A., & Rubin, R. L. (2012). Increased plant productivity in Alaskan tundra as a result of experimental warming of soil and permafrost. *Journal of Ecology*, 100(2), 488-498.
- Nemani, R. R., Keeling, C. D., Hashimoto, H., Jolly, W. M., Piper, S. C., Tucker, C. J., . . . Running, S. W. (2003). Climate-driven increases in global terrestrial net primary production from 1982 to 1999. *Science*, 300(5625), 1560-1563.
- Olson, D. M., Dinerstein, E., Wikramanayake, E. D., Burgess, N. D., Powell, G. V., Underwood, E. C., . . . Morrison, J. C. (2001). *Terrestrial Ecoregions of the World: A New Map of Life on Earth: A new global map of terrestrial ecoregions provides an innovative tool for conserving biodiversity*. *Bioscience*, 51(11), 933-938.

- Park, T., Ganguly, S., Tømmervik, H., Euskirchen, E. S., Høgda, K.-A., Karlsen, S. R., . . . Myneni, R. B. (2016). Changes in growing season duration and productivity of northern vegetation inferred from long-term remote sensing data. *Environmental Research Letters*, 11(8), 084001.
- Parmesan, C., & Yohe, G. (2003). A globally coherent fingerprint of climate change impacts across natural systems. *Nature*, 421(6918), 37.
- Pastorello, G., Papale, D., Chu, H., Trotta, C., Agarwal, D., Canfora, E., ... & Torn, M. (2017). A new data set to keep a sharper eye on land-air exchanges. *Eos, Transactions American Geophysical Union (Online)*, 98(8).
- Peng, C., Ma, Z., Lei, X., Zhu, Q., Chen, H., Wang, W., ... & Zhou, X. (2011). A drought-induced pervasive increase in tree mortality across Canada's boreal forests. *Nature climate change*, 1(9), 467.
- Piao, S., Ciais, P., Friedlingstein, P., Peylin, P., Reichstein, M., Luysaert, S., . . . Chen, A. (2008). Net carbon dioxide losses of northern ecosystems in response to autumn warming. *Nature*, 451(7174), 49-52.
- Piao, S., Liu, Z., Wang, T., Peng, S., Ciais, P., Huang, M., . . . Janssens, I. A. (2017). Weakening temperature control on the interannual variations of spring carbon uptake across northern lands. *Nature Climate Change*, 7(5), 359-363.
- Prentice, I. C., Cramer, W., Harrison, S. P., Leemans, R., Monserud, R. A., & Solomon, A. M. (1992). Special paper: a global biome model based on plant physiology and dominance, soil properties and climate. *Journal of Biogeography*, 117-134.
- Pulliainen, J., Aurela, M., Laurila, T., Aalto, T., Takala, M., Salminen, M., . . . Laaksonen, A. (2017). Early snowmelt significantly enhances boreal springtime carbon uptake. *Proceedings of the National Academy of Sciences*, 114(42), 11081-11086.

- Accepted Article
- Randerson, J., Field, C., Fung, I., & Tans, P. (1999). Increases in early season ecosystem uptake explain recent changes in the seasonal cycle of atmospheric CO₂ at high northern latitudes. *Geophysical Research Letters*, 26(17), 2765-2768.
- Reich, P. B., Sendall, K. M., Stefanski, A., Rich, R. L., Hobbie, S. E., & Montgomery, R. A. (2018). Effects of climate warming on photosynthesis in boreal tree species depend on soil moisture. *Nature*, 562(7726), 263.
- Richardson, A. D., Black, T. A., Ciais, P., Delbart, N., Friedl, M. A., Gobron, N., ... & Migliavacca, M. (2010). Influence of spring and autumn phenological transitions on forest ecosystem productivity. *Philosophical Transactions of the Royal Society of London B: Biological Sciences*, 365(1555), 3227-3246.
- Richardson, A. D., Keenan, T. F., Migliavacca, M., Ryu, Y., Sonnentag, O., & Toomey, M. (2013). Climate change, phenology, and phenological control of vegetation feedbacks to the climate system. *Agricultural and Forest Meteorology*, 169, 156-173.
- Rodell, M., Houser, P., Jambor, U., Gottschalck, J., Mitchell, K., Meng, C., . . . Bosilovich, M. (2004). The global land data assimilation system. *Bulletin of the American Meteorological Society*, 85(3), 381-394.
- Rödenbeck, C., Houweling, S., Gloor, M., & Heimann, M. (2003). CO₂ flux history 1982–2001 inferred from atmospheric data using a global inversion of atmospheric transport. *Atmospheric Chemistry and Physics*, 3(6), 1919-1964.
- Rogers, A., Medlyn, B.E., Dukes, J.S., Bonan, G., Von Caemmerer, S., Dietze, M.C., . . . Prentice, I.C. (2017). A roadmap for improving the representation of photosynthesis in Earth system models. *New Phytologist*, 213(1), 22-42.
- Rossi, S., Deslauriers, A., Anfodillo, T., Morin, H., Saracino, A., Motta, R., . . . Borghetti, M. (2006). Conifers in cold environments synchronize maximum growth rate of tree ring formation with day length. *New phytologist*, 170(2), 301-310.

- Rotenberg, E., & Yakir, D. (2010). Contribution of semi-arid forests to the climate system. *Science*, 327(5964), 451-454.
- Running, S., Mu, Q., & Zhao, M. (2015). MOD17A2H MODIS/Terra Gross Primary Productivity 8-Day L4 Global 500m SIN Grid V006. NASA EOSDIS Land Processes DAAC.
- Smith, N.G., Malyshev, S.L., Shevliakova, E., Kattge, J., & Dukes, J.S. (2016). Foliar temperature acclimation reduces simulated carbon sensitivity to climate. *Nature Climate Change*, 6(4), 407.
- Sprengel, C. (1828). Von den Substanzen der Ackerkrume und des Untergrundes (About the substances in the plow layer and the subsoil). *Journal for Technische and Okonomische Chemie*, 2, 397-421.
- Taylor, K. E., Stouffer, R. J., & Meehl, G. A. (2012). An overview of CMIP5 and the experiment design. *Bulletin of the American Meteorological Society*, 93(4), 485-498.
- Thomson, A. M., Calvin, K. V., Smith, S. J., Kyle, G. P., Volke, A., Patel, P., . . . Clarke, L. E. (2011). RCP4. 5: a pathway for stabilization of radiative forcing by 2100. *Climatic Change*, 109(1-2), 77.
- Thoning, K. W., Tans, P. P., & Komhyr, W. D. (1989). Atmospheric carbon dioxide at Mauna Loa Observatory: 2. Analysis of the NOAA GMCC data, 1974–1985. *Journal of Geophysical Research: Atmospheres*, 94(D6), 8549-8565.
- Vautard, R., Yiou, P., & Ghil, M. (1992). Singular-spectrum analysis: A toolkit for short, noisy chaotic signals. *Physica D: Nonlinear Phenomena*, 58(1-4), 95-126.
- Walther, G. R. (2010). Community and ecosystem responses to recent climate change. *Philosophical Transactions of the Royal Society of London B: Biological Sciences*, 365(1549), 2019-2024.

- Accepted Article
- Welp, L. R., Patra, P. K., Rödenbeck, C., Nemani, R., Bi, J., Piper, S. C., & Keeling, R. F. (2016). Increasing summer net CO₂ uptake in high northern ecosystems inferred from atmospheric inversions and comparisons to remote-sensing NDVI. *Atmospheric Chemistry and Physics*, 16(14), 9047-9066.
- Xia, J., Niu, S., Ciais, P., Janssens, I. A., Chen, J., Ammann, C., . . . Bonal, D. (2015). Joint control of terrestrial gross primary productivity by plant phenology and physiology. *Proceedings of the National Academy of Sciences*, 112(9), 2788-2793.
- Xu, L., Myneni, R., Chapin Iii, F., Callaghan, T., Pinzon, J., Tucker, C., . . . Tømmervik, H. (2013). Temperature and vegetation seasonality diminishment over northern lands. *Nature Climate Change*, 3(6), 581-586.
- Yamori, W., Hikosaka, K., & Way, D.A. (2014). Temperature response of photosynthesis in C₃, C₄, and CAM plants: temperature acclimation and temperature adaptation. *Photosynthesis research*, 119(1-2), 101-117.
- Zhang, Y., Guanter, L., Berry, J. A., Joiner, J., van der Tol, C., Huete, A., ... & Köhler, P. (2014). Estimation of vegetation photosynthetic capacity from space-based measurements of chlorophyll fluorescence for terrestrial biosphere models. *Global Change Biology*, 20(12), 3727-3742.
- Zhao, F., & Zeng, N. (2014). Continued increase in atmospheric CO₂ seasonal amplitude in the 21st century projected by the CMIP5 Earth system models. *Earth System Dynamics*, 5(2), 423.
- Zhao, M., Heinsch, F. A., Nemani, R. R., & Running, S. W. (2005). Improvements of the MODIS terrestrial gross and net primary production global data set. *Remote Sensing of Environment*, 95(2), 164-176.

Zhou, S., Zhang, Y., Ciais, P., Xiao, X., Luo, Y., Caylor, K. K., ... & Wang, G. (2017).

Dominant role of plant physiology in trend and variability of gross primary productivity in North America. *Scientific Reports*, 7, 41366.

FIGURE CAPTION

Figure 1. Conceptual illustration of the proposed DOY_{Pmax} framework. Seasonal cycle of temperature (T, red), radiation (R, green), water availability (W, blue) and GPP (P, black) over common northern terrestrial ecosystems. Vertical lines indicate when each variable reaches a maximum state. DOY_{Pmax} , DOY_{Tmax} , DOY_{Rmax} , and DOY_{Wmax} stand for the day of year when GPP, temperature, radiation and precipitation reach respective maximum state during each seasonal course of the year. Four idealized cases are shown to demonstrate how photosynthetic seasonality of the ecosystem under given climate constraint differs from each other: non- (solid line, Case 1), temperature- (dotdash line, Case 2), water- (longdash line, Case 3), and radiation- (solid line, Case 4) constrained ecosystems.

Figure 2. Relative positioning of peak photosynthetic activity timing with respect to the seasonal course of temperature and radiation, and its relation to climatic constraints and productivity. (a) Geographical distribution of $\delta DOY_{P,T}$ ($DOY_{Pmax} - DOY_{Tmax}$) and $\delta DOY_{P,R}$ ($DOY_{Pmax} - DOY_{Rmax}$) for northern ecosystems. Regional distribution of $\delta DOY_{P,T}$ and $\delta DOY_{P,R}$ over Arctic (AR), Boreal (BO) and Temperate (TE) regions is given in the inset violin plot with mean and 1 SD (bracket). (b) Positioning of DOY_{Pmax} seen as the relation between $\delta DOY_{P,R}$ and $\delta DOY_{P,T}$, with respect to temperature ($^{\circ}C$). (c) Same as b but for water

availability (i.e., RAP). **(d)** Same as **b** but for GPP_{Total} ($kg\ C\ m^{-2}$). MODIS-derived outcomes are used for these panels.

Figure 3. **(a)** Same as Figure 2a but for the independent satellite Sun-Induced Fluorescence (SIF). **(b)-(d)** Same as Figure 2b-d but for the eddy covariance tower measurement. Total 92 FLUXNET sites (Figure S2a) were used and each dot represents a single site.

Figure 4. Spatial pattern of changes in DOY_{Pmax} and temperature during last 17 years (2000 – 2016). **(a)** Decadal trend of MODIS based DOY_{Pmax} over northern land during last 17 years. **(b)** Same as **a** but for summer temperature (June – August). The trend was derived based on ordinary least squares regression.

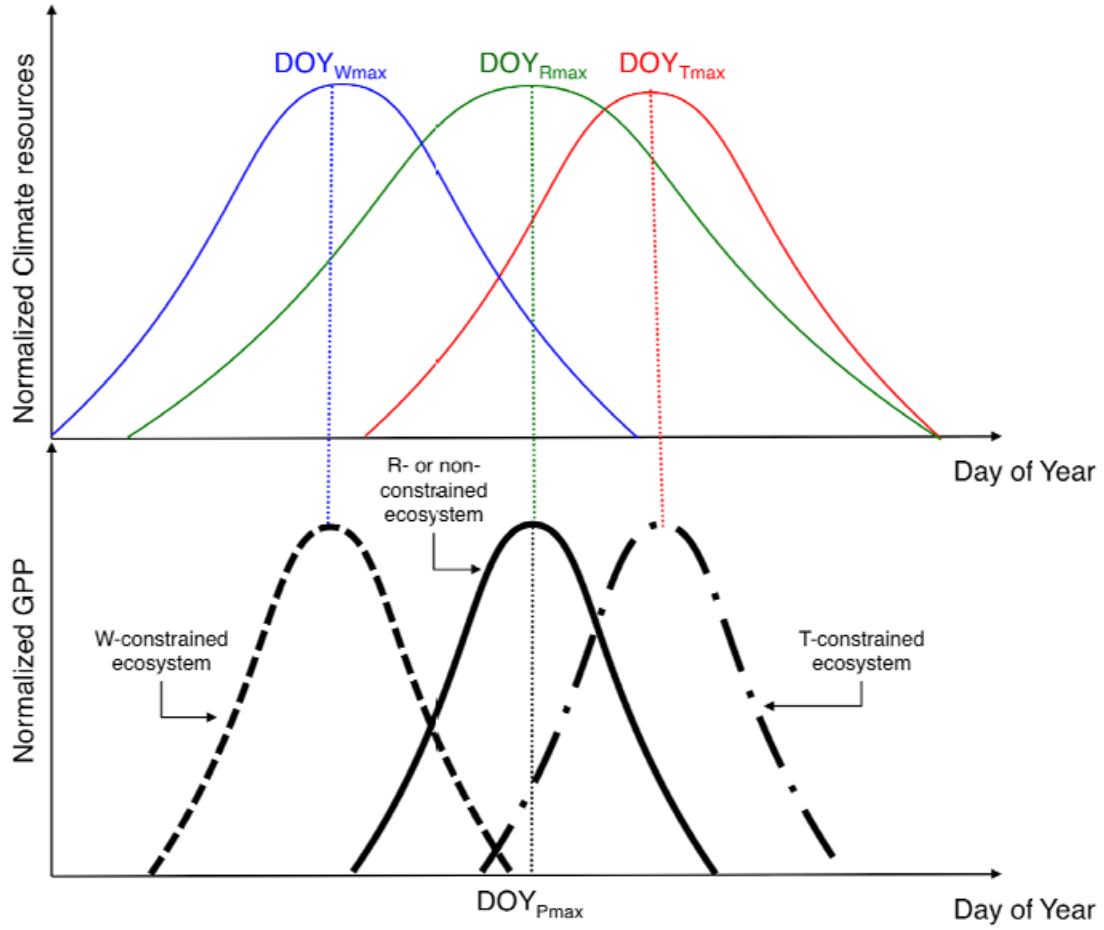
Figure 5. Changes in DOY_{Pmax} during last 17 years (2000 – 2016) and their implications on northern vegetation productivity. **(a)** Inter-annual variation of DOY_{Pmax} by regions (Arctic: AR, Boreal: BO, Temperate: TE, Northern Hemisphere: NH) and its trend over last 17 years. The decadal trend is estimated based on the 5-year moving average approach to reduce the potential impact of first, last and outlier points. Thin solid line with markers and thick solid line represent annual DOY_{Pmax} and 5-year moving average. Calculated trend (slope \pm SE) based on ordinary least squares regression is given with its significance level (double asterisks denote $P < 0.001$, single asterisks denote $P < 0.05$). The significance was computed by using the non-parametric Mann-Kendall trend test. **(b)** Relation between regional DOY_{Pmax} and summer temperature (June – August) anomalies. **(c)–(d)** Same as **b** but for respective relation between DOY_{Pmax} and GPP_{Total} , and DOY_{Pmax} and GPP_{Ratio} anomalies.

Significance of the slope estimate ($\beta \pm SE$) is denoted as double ($P < 0.001$) and single ($P < 0.05$) asterisks. The Kendall's rank correlation coefficient (r) between two variables is also given. Dark blue, light blue, green and gray stand for AR, BO, TE and NH, respectively.

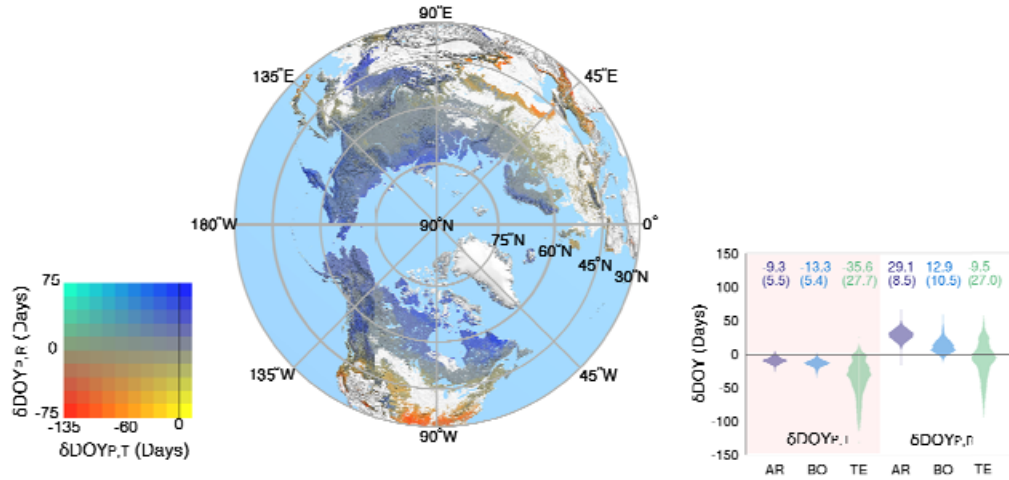
Figure 6. Analysis of atmospheric CO₂ concentration at Point Barrow and two CO₂ inversion estimates. (a) Time series of DOY_{Zero-Crossing} observed at Point Barrow atmospheric observatory and two independent CO₂ inversion datasets (CAMS and JENA). Note that the CO₂ fluxes for DOY_{Zero-Crossing} retrieval of the inversion datasets are based on regionally integrated fluxes over the arctic and boreal zones, and all trend estimates are based on the 5-year moving average approach. Calculated trend (slope \pm SE) based on ordinary least squares regression is given with its significance level (double asterisks denote $P < 0.001$, single asterisks denote $P < 0.05$). The significance was computed by using the non-parametric Mann-Kendall trend test. (b) Relation between DOY_{Zero-Crossing} and seasonal cycle amplitude (SCA) of atmospheric CO₂ concentration and flux estimates. SCA anomaly was expressed as percentage of long-term mean. Significance of the slope estimate ($\beta \pm SE$) is denoted as double ($P < 0.001$) and single ($P < 0.05$) asterisks. The Kendall rank correlation coefficient (r) was used to measure degree of association. Red, blue, and green stand for CO₂ data from Point Barrow, CAMS, and JENA, respectively.

Figure 7. Analysis of multiple CMIP5 ESMs during two separate periods: (a) 1980-2030 and (b) 2050-2100. Decadal trend of DOY_{Pmax} (left) and its association to GPP_{Total} (center) and GPP_{Ratio} (right) over northern lands inferred from the seven ESMs. Bar charts with error bars depict mean \pm 1 SD across all ESMs. The Kendall rank correlation coefficient (r) was

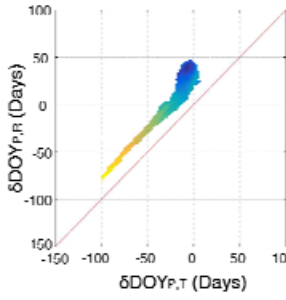
used to measure degree of association. Dark blue, light blue, green and gray stand for AR, BO, TE and NH, respectively.



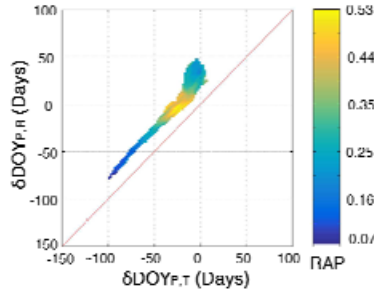
a



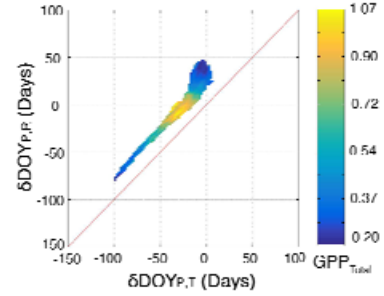
b

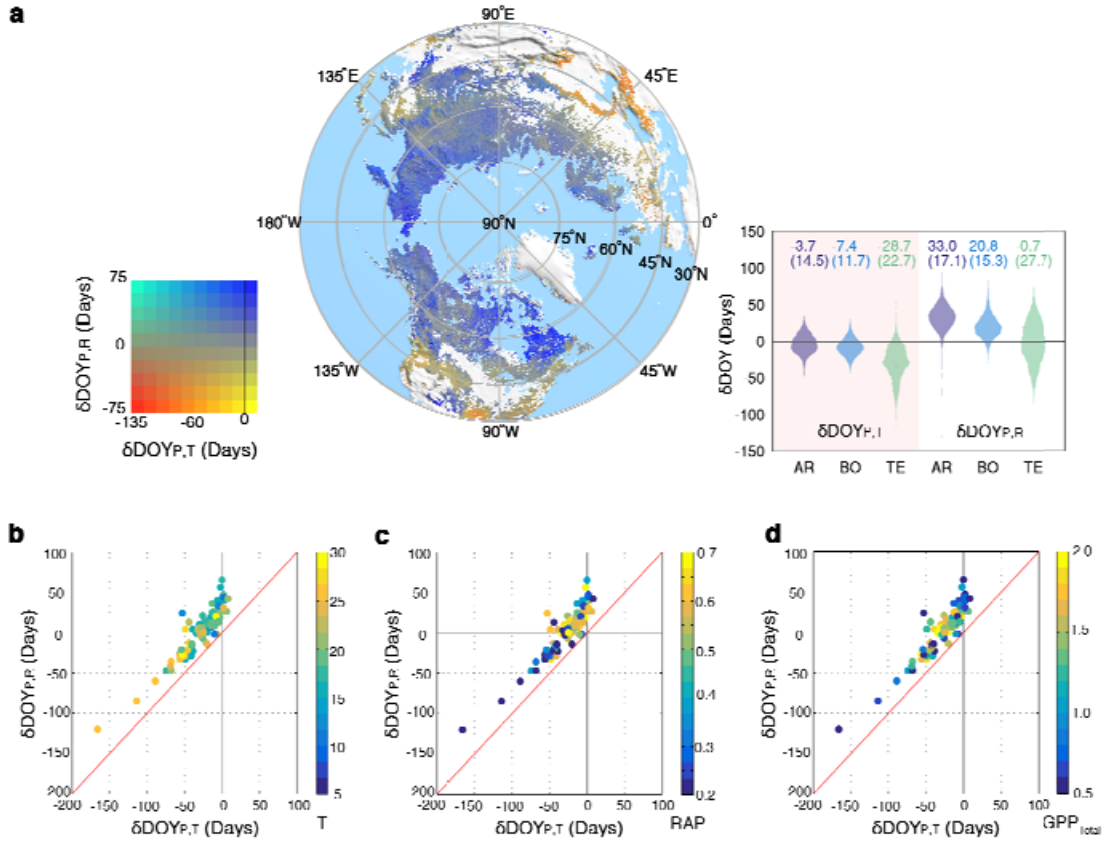


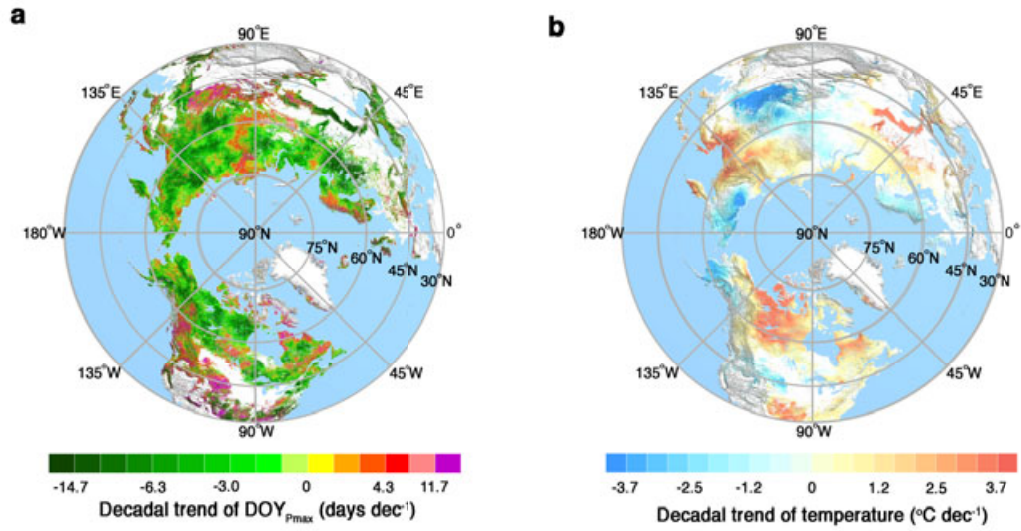
c



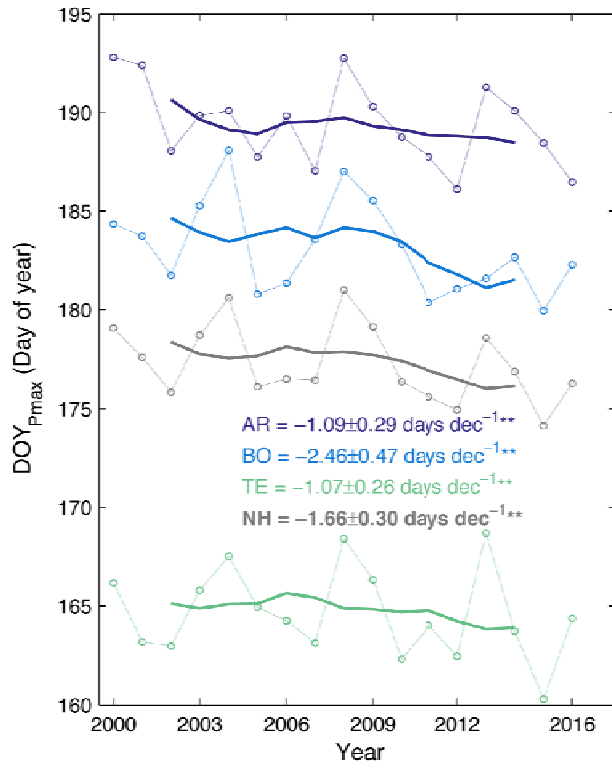
d



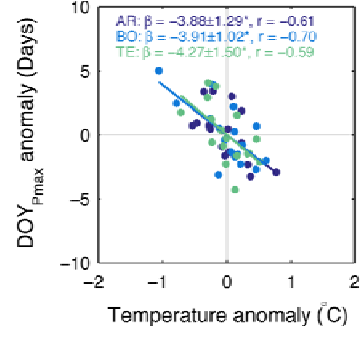




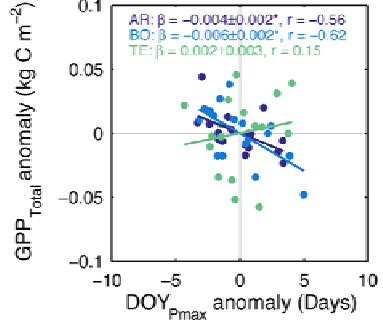
a



b



c



d

